ADVANCED BIOLOGY
www.advanced-bio.com

# Micropatterned Surfaces Expose the Coupling between Actin Cytoskeleton-Lamin/Nesprin and Nuclear Deformability of Breast Cancer Cells with Different Malignancies

*Ezgi Antmen, Utkan Demirci, and Vasif Hasirci**

**Mechanotransduction proteins transfer mechanical stimuli through nucleo-cytoskeletal coupling and affect the nuclear morphology of cancer cells. However, the contribution of actin filament integrity has never been studied directly. It is hypothesized that differences in nuclear deformability of cancer cells are influenced by the integrity of actin filaments. In this study, transparent micropatterned surfaces as simple tools to screen cytoskeletal and nuclear distortions are presented. Surfaces decorated with micropillars are used to culture and image breast cancer cells and quantify their deformation using shape descriptors (circularity, area, perimeter). Using two drugs (cytochalasin D and jasplakinolide), actin filaments are disrupted. Deformation of cells on micropillars is decreased upon drug treatment as shown by increased circularity. However, the effect is much smaller on benign MCF10A than on malignant MCF7 and MDAMB231 cells. On micropatterned surfaces, molecular analysis shows that Lamin A/C and Nesprin-2 expressions decreased but, after drug treatment, increased in malignant cells but not in benign cells. These findings suggest that Lamin A/C, Nesprin-2 and actin filaments are critical in mechanotransduction of cancer cells. Consequently, transparent micropatterned surfaces can be used as image analysis platforms to provide robust, high throughput measurements of nuclear deformability of cancer cells, including the effect of cytoskeletal elements.**

## 1. Introduction

All cells are continuously exposed to mechanical forces created by the extracellular environment and they can sense and respond to these forces through mechanotransduction. Mechanotransduction is the process by which cells convert mechanical stimuli into biochemical signals.[1] Mechanotransduction has a role in the regulation of blood pressure, remodeling of bone, maintenance of muscle, perception of touch and sound, cell growth, migration, gene expression, morphological changes, proliferation and differentiation as well as tissue morphogenesis and the pathogenesis of various diseases, such as cardiovascular diseases, osteoporosis, and cancer.[2] During force transmission through a cell, constant reorganization of the cell interior is needed, and this reorganization is realized by cytoskeletal remodeling and directed by mechanosensitive signaling pathways. The structural link between the cytoskeleton and nucleus plays an important role in this force transmission and it is referred to as the nucleo-cytoskeleton

Dr. E. Antmen, Prof. V. Hasirci
BIOMATEN
Middle East Technical University (METU)
Center of Excellence in Biomaterials and Tissue Engineering
Ankara, 06800, Turkey
E-mail: Vasif.Hasirci@acibadem.edu.tr
Dr. E. Antmen, Prof. V. Hasirci
Department of Biotechnology
Middle East Technical University (METU)
Ankara, 06800, Turkey
Prof. U. Demirci
Bio-Acoustic-MEMS in Medicine (BAMM) Laboratory
Canary Center at Stanford for Cancer Early Detection
Department of Radiology
Stanford University School of Medicine
Palo Alto, CA 94304, USA
Prof. U. Demirci
Department of Radiology
School of Medicine
Stanford University
Palo Alto, CA 94304, USA
Prof. V. Hasirci
Department of Biological Sciences
Middle East Technical University (METU)
Ankara, 06800, Turkey
Prof. V. Hasirci
Department of Medical Engineering
Acibadem Mehmet Ali Aydinlar University
Atasehir, Istanbul 34752, Turkey
The ORCID identification number(s) for the author(s) of this article can be found under https://doi.org/10.1002/adbi.202000048.

**DOI: 10.1002/adbi.202000048**

 

coupling. Through this coupling, cell surface forces and substrate rigidity can change nuclear morphology and external forces can be transmitted to the nucleus and change chromosome movement and nuclear positioning. Actin filament networks of the cytoskeleton, as one of the most important components of nucleo-cytoskeleton coupling, play a critical role in maintenance of the form and orientation of nuclei, nuclear morphology, and cellular stiffness through their polymerization and depolymerization.[3,4] In cancer studies, understanding of force transmission has been gaining importance because increased actomyosin contractility can induce cell proliferation, extracellular matrix (ECM) remodeling, ECM stiffening, invasion and metastasis of tumor cells.[5] Tumor cells are known to alter their own mechanical properties and change their responses to external physical cues. Thus, the development and metastasis of cancer are closely regulated by mechanical stresses applied on the cytoskeleton and nucleus and their responses to these forces. On the other hand, nucleus is the main component of a cell which regulates the gene expression and protein synthesis.[6] It is also known that the nucleus is the major obstacle of a cell in migration through confined openings since it is the main contributor to the total cell stiffness, it is also the largest organelle of a cell and almost an order of magnitude stiffer than the cytoplasm.[7–9] Thus, nucleus of a metastatic or migrating cell has to be softer and must be able to deform more than the nuclei of the other cells. Supporting this, it was reported that knockdown of the expression of nuclear envelop protein, lamin A, causes a decrease in nuclear stiffness and increases cell motility and ability to migrate.[10,11]

Because force transmission through a cell is important in the migration and metastasis of a cancer cell, modifications in surface features of the substrate have been widely used in in vitro cell biology studies to manipulate cell responses to the external forces or to give surfaces cell discrimination capabilities. Creation of substrate surfaces with topographic features is one of the most commonly used surface modification approach to study the cell–substrate interactions. The topographies either mimic sizes and shapes of features found in the natural environment of cells or they have artificial geometries designed for specific reasons. Since the size of cells, adhesion proteins and their ligands are in the nanometer to micrometer scale, modifications at this level are required on the substrates to create the architecture that could mimic the ECM of a cell. Common shapes used in the fabrication of surface topographies are pores, gratings, wells, pits, cones, posts, pillars, grooves, or mesh-like structures that can be organized in a regular pattern.[12–16] Several studies have shown that many cell types react strongly to micro and nano features on substrate surfaces.[13–19] On such surfaces, changes have been reported in the cell behavior such as adhesion,[20,21] alignment,[21–23] morphology (cytoskeletal organization),[17,24] proliferation,[25] viability,[26] gene expression and differentiation.[14,27,28]

In this study, our assumption was that the differences in the malignancies of breast cancer cells are the result of the differences in their nuclear deformation. Based on this assumption, our hypothesis was that the level of completeness of polymerization of actin filaments can affect nuclear deformability and the metastatic capability of the cancer cells. Although it has been reported that biomechanical properties of the cell and nucleus give information about the state of cancer progression,[29,30] the interaction between the components of mechanotransduction complex (linkers of nucleoskeleton and cytoskeleton proteins (LINC), nuclear envelope proteins, actin filaments) and deformation of a nucleus has never been directly measured. The aim of this study was to explore the relation between the proteins of mechanical force transmission, nuclear deformability, and level of malignancy of a tumor cell by inhibiting the polymerization and depolymerization of actin cytoskeleton. Three breast cancer cell lines with different malignancy levels (benign MCF10A, malignant but noninvasive MCF7, malignant and highly invasive MDAMB231) were used to compare nuclear deformability and behavior (spreading, attachment) of these cells and expression of their nuclear membrane proteins on micropatterned surfaces to support our hypothesis. Cells were seeded on polymethyl methacrylate (PMMA) surfaces decorated with square prism pillars ($4 \times 4$ μm$^2$ surface area, 4 μm gap size, and 8 μm height). Two different drugs, selective for actin and inhibit its polymerization, were used: Cytochalasin D (inhibits actin polymerization by capping filaments that bind to monomers) and Jasplakinolide (prevents actin depolymerization, forms actin aggregates, and blocks focal adhesion kinase (FAK) signaling). Also, the relation between the deformability of nucleus, inhibition of actin polymerization, and the expression of Lamin A/C and Nesprin-2 was investigated.

## 2. Experimental Section

### 2.1. Preparation of Micropatterned PMMA Films

Micropillar arrays were designed at METU BIOMATEN and outsourced to be fabricated using photolithography.[13,15,16] The micropillars were in square prism shape, 8 $\mu$m tall with $4 \times 4$ $\mu$m$^2$ area and 4 $\mu$m interpillar gap. Using wafers as a template, polydimethylsiloxane (PDMS) molds were prepared with Sylgard 184 silicone prepolymer and Sylgard 184 curing agent (Dow Corning Company, UK) (10:1 w/w) and cured for 4 h at 70 °C. PMMA films (Mw ≈ 996 kDa) (Sigma, Germany) were made by solvent removal from a solution (10% w/v in chloroform) on the PDMS mold which was air-dried for 12 h at room temperature. As a control, smooth PDMS molds were used to obtain smooth PMMA films.

### 2.2. Characterization of PMMA Films

After coating with Au/Pd under vacuum, surface patterns of the PMMA films were examined with scanning electron microscopy (SEM) (400F Field Emission SEM, USA).

### 2.3. In Vitro Studies

#### *2.3.1. Culture of Breast Cancer Cell Lines*

MCF-10A cells were cultured in DMEM/F12 medium (Sigma, USA) supplemented with 5% fetal bovine serum (FBS) (Lonza, USA), EGF 20 ng mL$^{-1}$ (Sigma), insulin 10 $\mu$g mL$^{-1}$ (Sigma), hydrocortisone 0.5 mg mL$^{-1}$ (Sigma), cholera toxin 100 ng mL$^{-1}$ (Sigma), and 100 units mL$^{-1}$ penicillin (Sigma, USA). MCF-7 cells were cultured in DMEM low glucose medium (Lonza, USA) supplemented with 10% FBS (Lonza, USA) and 100 U mL$^{-1}$

 

penicillin (Sigma, USA). MDA-MB-231 cells were cultured in DMEM high glucose medium (Lonza, USA) supplemented with 10% FBS (Lonza, USA) and 100 U $mL^{-1}$ penicillin (Sigma, USA).

PMMA films were sterilized by UV for 15 min. Cells were seeded at a density of $5 \times 10^4$ cells/film in 100 $\mu$L of their specific growth medium, left for 6 h for adhesion at 37 °C, 5% $CO_2$. Tissue culture plates (TCPS) and smooth (S) PMMA films were used as controls.

#### 2.3.2. Testing of Actin Inhibitor Drugs

*Dose Optimization with Alamar Blue Assay*: Two different drugs (Cytochalasin D and Jasplakinolide) were used and solutions of both drugs in dimethyl sulfoxide (DMSO) were prepared. Final concentrations of both drugs in 1 mL of culture medium were in the range 0.01–10 × $10^{-6}$ M for Cytochalasin D and 0.01–5 × $10^{-6}$ M for Jasplakinolide. Control samples without drugs were prepared with the same highest amount of DMSO for both drugs. Cells were cultured for 24 h (day 1) in TCPS and on micropatterned films (P), and then drugs were used on the cells for another 24 h (day 2). The half maximal inhibitory concentration (IC50) of Cytochalasin D and Jasplakinolide on the cell viability before and after drug treatment was determined by Alamar Blue assay. Effect of these chemicals on prevention of nuclear deformation of three cell lines was observed and quantified under fluorescence microscopy.

### 2.4. Microscopy Studies

#### 2.4.1. Fluorescence Microscopy

Cell seeded samples were fixed in 4% paraformaldehyde, permeabilized with 1% Triton-X 100 solution (Applichem, Germany), and incubated in BSA blocking solution (1% w/v, in phosphate buffered saline (PBS)) at 37 °C for 30 min. Then, films were incubated in Alexa Fluor 488 labeled Phalloidin solution (1:50, in 0.1% BSA in PBS) for 1 h, 37 °C, and then DAPI (1:1000, in 0.1% BSA in PBS) (Invitrogen, USA) was used for 5 min at room temperature to stain the nuclei. Fluorescence microscopy images were obtained with an upright fluorescence microscope (Zeiss Axio Imager M2, Germany). The images were obtained by using black and white filter of the microscope and pseudocolored with green (actin) and red (nucleus) by the software system of the microscope.

#### 2.4.2. Confocal Microscopy for Immunocytochemistry (ICC)

Confocal microscopy images of the cells were obtained using an upright confocal laser scanning microscope (CLSM) using 488, 532, and 630 nm lasers (Leica SPE, Germany). Samples were fixed, permeabilized, and blocked in the same way in the previous section. Then, they were incubated for 1 h at 37 °C with Alexa Fluor 532 Phalloidin (Invitrogen, USA) to stain the actin cytoskeleton. For Lamin A/C and Nesprin-2, the antibodies specific to these proteins (Anti-Nesprin-2 ab57397 and anti-Lamin-A ab8980, Abcam, UK) were used according to manufacturer's directions. TOPRO-3 (1:1000, in PBS) (Invitrogen, USA) was used for 15 min at room temperature to stain the nuclei.

Details of imaging process and microscopy settings were presented in Figure S1 (Supporting Information).

### 2.5. Digital Analysis of Microscopy Images

#### 2.5.1. Quantification of Nuclear Deformation

Fluorescence microscopy images of the nuclei of cells were analyzed by using the image analysis software ImageJ (NIH)[31] to determine the "circularity" (Equation (1)) of cell nuclei

$$\text{Circularity} = 4\pi \times ([A]) / ([P]^2) \quad (1)$$

where $A$ is the area and $P$ is the perimeter of the nuclei.

Analyses were performed using 100 cell nuclei per surface. For the autothresholding of the images, ImageJ was used.[32]

A "circularity" value of 1 indicates a perfect circle. As the value decreases towards 0, the shape becomes an increasingly elongated polygon. Steps for the quantification of nuclei on smooth and micropatterned surfaces were presented in Figure S2 (Supporting Information).

### 2.6. Quantification of Expression Levels of Proteins Based on the Intensity of ICC Staining

Confocal microscopy Images of the samples stained with antibodies specific to Lamin A/C and Nesprin-2 were analyzed by using image analysis software Fiji.[33] Original images were in red (R), green (G), blue (B) format. Image preprocessing was applied to obtain gray scale (8 bit) images. "Lookup table" of Fiji was changed to "HiLo". Then the contrast was adjusted. Background subtraction was done using "rolling ball algorithm".[34] Finally, the intensity of the antibody specific stain was measured and a mean gray value (sum of the gray values of all the pixels in the selection divided by the number of pixels) was obtained for each image. Protocol for the quantification of signal intensity obtained from the imaging of protein expressions of the cells was presented in Figure S3 (Supporting Information).

### 2.7. Quantification of Protein Expression Levels with Western Blot Analysis

M-PER Mammalian Protein Extraction Reagent (Thermo Fisher Scientific) consisting of 1× protease and phosphatase inhibitors (Roche) was used for the isolation of whole cell extract in accordance with manufacturer's instructions. Proteins were isolated from the nuclear and cytoplasmic fractions. First, the cells were washed twice with PBS and then lysed in 300 µL of a hypotonic buffer containing $10 \times 10^{-3}$ M HEPES (pH 7.5), $4 \times 10^{-3}$ M NaF, $10 \times 10^{-6}$ M $Na_2MoO_4$, $0.1 \times 10^{-3}$ M EDTA, 1× protease and phosphatase inhibitors (Roche) and incubated on ice for 15 min. Then, 75 $\mu$L of 10% NP-40 (Pan-Reac AppliChem, Darmstadt, Germany) was added and mixed with pipetting. Then,

supernatants containing the cytoplasmic fraction were obtained by pulse centrifugation at 14 000 *g* for 30 s at 4 °C. Supernatant containing cytoplasmic proteins was transferred to a new Eppendorf tube. Remaining nuclear pellet was resuspended in 80 $\mu$L of nuclear extraction buffer containing $10 \times 10^{-3}$ M HEPES, (pH 7.9), $0.1 \times 10^{-3}$ M EDTA, $1.5 \times 10^{-3}$ M $MgCl_2$, $420 \times 10^{-3}$ M NaCl, 10% glycerol, and with 1× protease and phosphatase inhibitors, incubated on ice on an orbital shaker and vortexed for 30 s at 15 min. The lysate was centrifuged for 10 min at 14 000 *g* at 4 °C. The supernatant contains the nuclear fraction.

Total protein amount was estimated using the colorimetric Micro BCA Protein Assay (Thermoscientific). Standard curve is presented in Figure S9 (Supporting Information). Total cytoplasmic (20 $\mu$g) and nuclear proteins (7 $\mu$g) and multicolor spectrum extended range protein ladder (Thermoscientific, Cat. No. 26634) were loaded and separated by size on 10% SDS-PAGE gels and transferred to preactivated PVDF membranes by Transfer Blot turbo system using manufacturer's protocol.

Before staining the bands, unspecific sites were blocked with 5% skim milk (Sigma) for 1 h at room temperature (RT). Primary antibody incubation was performed overnight at 4 °C using the following antibody concentrations: Lamin A/C (1:2500, AntiRabbit, Sigma, Cat. No. L1293), and Nesprin-2 (1:150, AntiRabbit, Abcam, Cat. No. ab233034) in 5% skim milk. After washing the membranes three times with Tris-buffered saline with Tween 20 (TBST) ($20 \times 10^{-3}$ M Tris, pH 7.5; $150 \times 10^{-3}$ M NaCl; 0.1% Tween 20), membrane blots were incubated with the secondary goat anti-rabbit IgG, HRP-linked antibody (1:2000 in 5% skim milk, Cell Signaling Technology, Cat. No.. 7074) for 1 h at RT. Protein bands were visualized with the 1× LumiGLO Reagent and 1× Peroxide (Cell Signaling Technology, Cat. No. 7003), and ChemiDoc MP Imaging System (Bio-Rad). Band intensities were normalized to housekeeping proteins and the results given as "fold change". HDAC1 (1:2500, Anti-Rabbit, Abcam, Cat. No. Ab7028) and GAPDH (1:2500, Anti-Rabbit, Abcam, Cat. No. Ab9485) in 5% skim milk were used as housekeeping proteins for nuclear and cytoplasmic extracts, respectively. Full-sized immunoblot images are given in Figure S10 (Supporting Information).

### 2.8. Statistical Analysis

All quantitative data in this study were expressed as mean ± standard deviations with $n \geq 3$ unless otherwise stated. For each analysis, five images from three different samples were used. Shape analyses were done with 100 cells per surface. Normality test on all collected data was performed by Shapiro–Wilk test. Statistical analysis was performed by one-way or two-way ANOVA (analysis of variance) test followed by Tukey's test for normally distributed data and Kruskal–Wallis test for non-normally distributed data. Data were presented as symbol plots, where symbols and error bars represent the mean and standard deviation, respectively, or presented as box-whisker plots, where boxes represent 25th and 75th percentiles and whiskers represent the values from min to max. The line in the middle of the box is plotted at the median and "+" at the mean. Statistical significance is set at 95% confidence level for all tests ($p < 0.05$).

## 3. Results and Discussions

Square prism shaped micropillar (8 $\mu$m tall, $4 \times 4$ $\mu m^2$ area, 4 $\mu$m interpillar gap) decorated surfaces (P) were prepared on PDMS using the original wafer as the main template. Unpatterned (smooth) (S) surfaces served as controls. **Figure 1** shows a scheme of the workflow in this study. Figure 1A presents SEM images of the micropillar decorated and smooth surfaces and their graphical illustrations (insets). Figure 1B shows the nuclear deformations of three breast cancer cell lines as quantified with the circularity value obtained by Fiji software and representative fluorescence microscopy images of their nuclei. Circularity values for the breast cancer cell lines are: 0.77 for benign MCF10A, 0.47 for noninvasive malignant MCF7, and 0.37 for invasive malignant MDAMB231. A high degree of nuclear deformation in the cells resulted in a lower circularity value. In our previous study, a detailed comparison of these three cell lines were made and it was shown that the nuclei of the more aggressive cancer cells have a higher capability of deformation.[16] This was also a proof of the ability of metastatic cancer cells migrate through dense ECM by changing the morphology of their nuclei.[35–38] Figure 1C shows the action mechanisms of the two actin inhibitor drugs Cytochalasin D (CytoD) and Jasplakinolide (Jasp) used in this study. CytoD binds to the positive end of the actin filaments and prevents their polymerization while Jasp binds to negative end and prevents depolymerization which results in aggregation of actin filaments.

### 3.1. Drug Testing on Breast Cancer Cells

Drugs inhibiting actin formation were used to study the role of mechanotransduction on the deformability of the cells because it is known that there is a coordination between the mechanosensory elements and force transmission.[39] External forces applied on a cell are transduced through the actin cytoskeleton to the nucleus and eventually may cause the deformability of the cell and its nucleus.[39] In the actin inhibiting drug tests, the cells were initially cultured for 24 h in the tissue culture plate, and then treated with the drugs for another 24 h before microscopy. Cytochalasin D used in this study inhibits actin polymerization by binding to the monomers and capping the filaments selectively.[40–42] Jasplakinolide, on the other hand, stimulates actin polymerization but disrupts F-actin fiber formation by blocking FAK signaling pathway.[43]

Dose–response curves show that when Cytochalasin D (CytoD) or Jasplakinolide (Jasp) (Figure S4, Supporting Information) were used at their highest concentration (10 and $5 \times 10^{-6}$ M, respectively), they decreased metabolic activity of the cells rather than completely stopping proliferation. This decrease was not more than 50% in most of the three cell types tested. In the literature, it was also shown that the cytotoxic levels of these drugs were above $100–200 \times 10^{-6}$ M against breast cancer cells and the concentrations used in our study were much more below the lethal dose.[42,43] Thus, the cells treated with the drugs were still showing metabolic activity.

Fluorescence microscopy images of the three cancer cells after interaction with the drugs on TCPS are shown in **Figure 2**. The cells were immunostained with Alexa Fluor 488 labeled Phalloidin (green) for filamentous actin (F-actin) and with

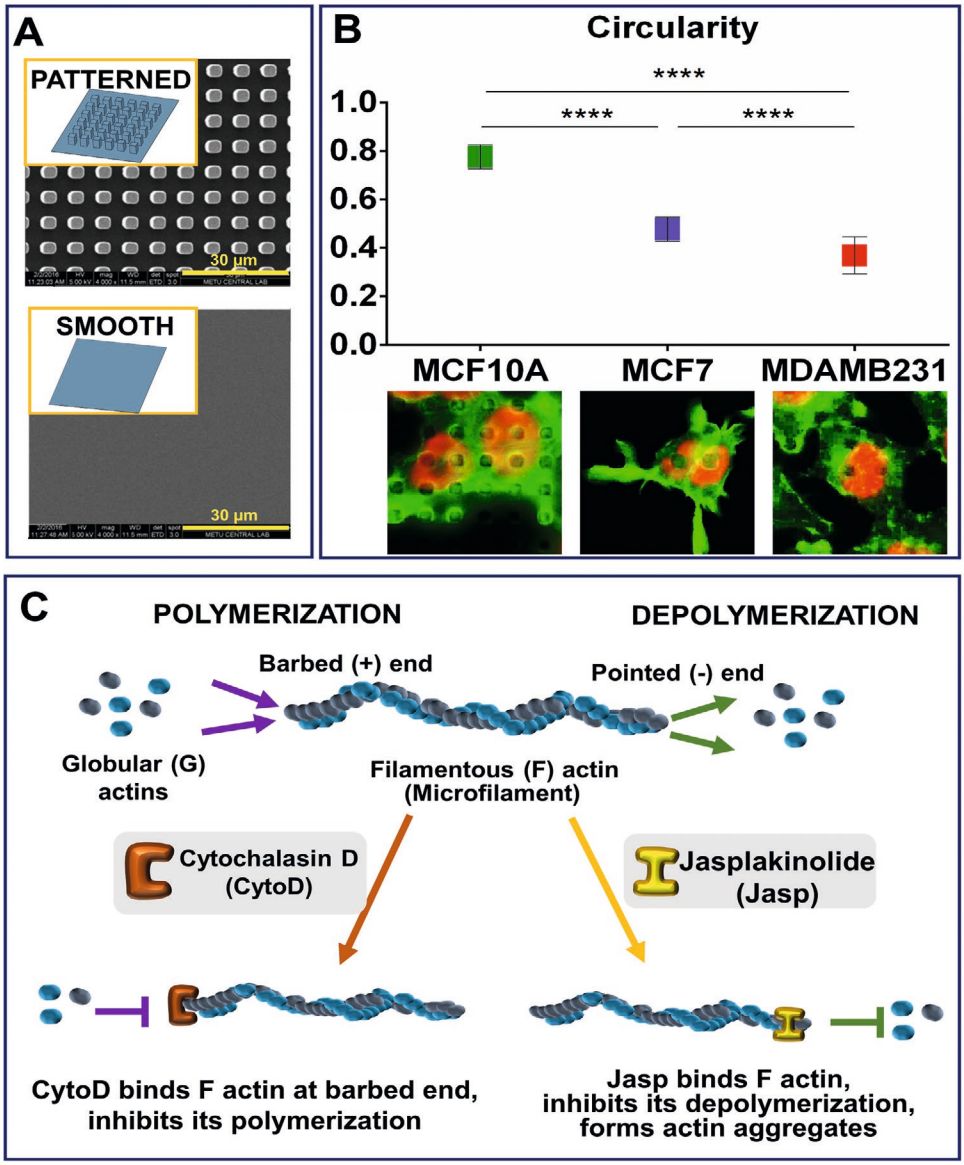


**Figure 1.** Summary of the nuclear deformability of cells on micropatterned surfaces and the action mechanism of the drugs inhibiting actins. A) SEM of patterned and smooth PMMA surfaces; B) Circularity value of three breast cancer cell lines (The distribution of shape descriptor values was non-normal and statistical analysis was carried out by Kruskal–Wallis nonparametric test, $n \geq 100$ cells/surface, $p < 0.0001$, $*p < 0.005$, $**p < 0.001$, $***p < 0.0005$, and $****p < 0.0001$. n.s: not significant); C) Acting mechanism of actin inhibitory drugs: CytoD and Jasp.

DAPI (red) for the nuclei. It is observed that increasing the concentration of drugs led to a progressive decrease in the actin contents as shown by the decrease in the green signal obtained from the actin-specific stain and disorganized and disrupted morphology of the actin cytoskeleton. Similar results were also shown in the literature that increasing CytoD concentration from 10 to 200 $\times 10^{-6}$ M resulted in progressive shrinking of the cells and reduced F-actin content when metastatic human cancer cell lines were used.[42]

In addition to the images of the cytoskeleton of the three cells, quantitative analysis of their cytoskeleton and nuclei with ImageJ (NIH) software are presented in **Figure 3**. Details of the image analysis are presented in Figure S5 (Supporting Information). Graphs display the analysis of area, perimeter and mean gray value analysis of actin cytoskeleton and area and perimeter of nuclei of the cells upon increasing drug concentrations. As deduced from the graphs, actin cytoskeletons and nuclei of all cells had decreasing values for all cytoskeletal parameters (area, perimeter, and mean gray value) with an increasing drug concentration as the indication of the actin disruption. Especially the highest concentrations of both drugs showed the most significant changes.

The highest concentrations of the both drugs ($10 \times 10^{-6}$ M for CytoD and $5 \times 10^{-6}$ M for Jasp) showed a distinct effect on the actins of the cells (Figure 2), so these two highest drug doses were selected to use in the nuclear deformation analysis.

Fluorescence microscopy images of the nuclei of the cells on micropatterned PMMA surfaces are presented in **Figure 4**. Upper two row images show cells after 24 and 48 h drug-free incubation.

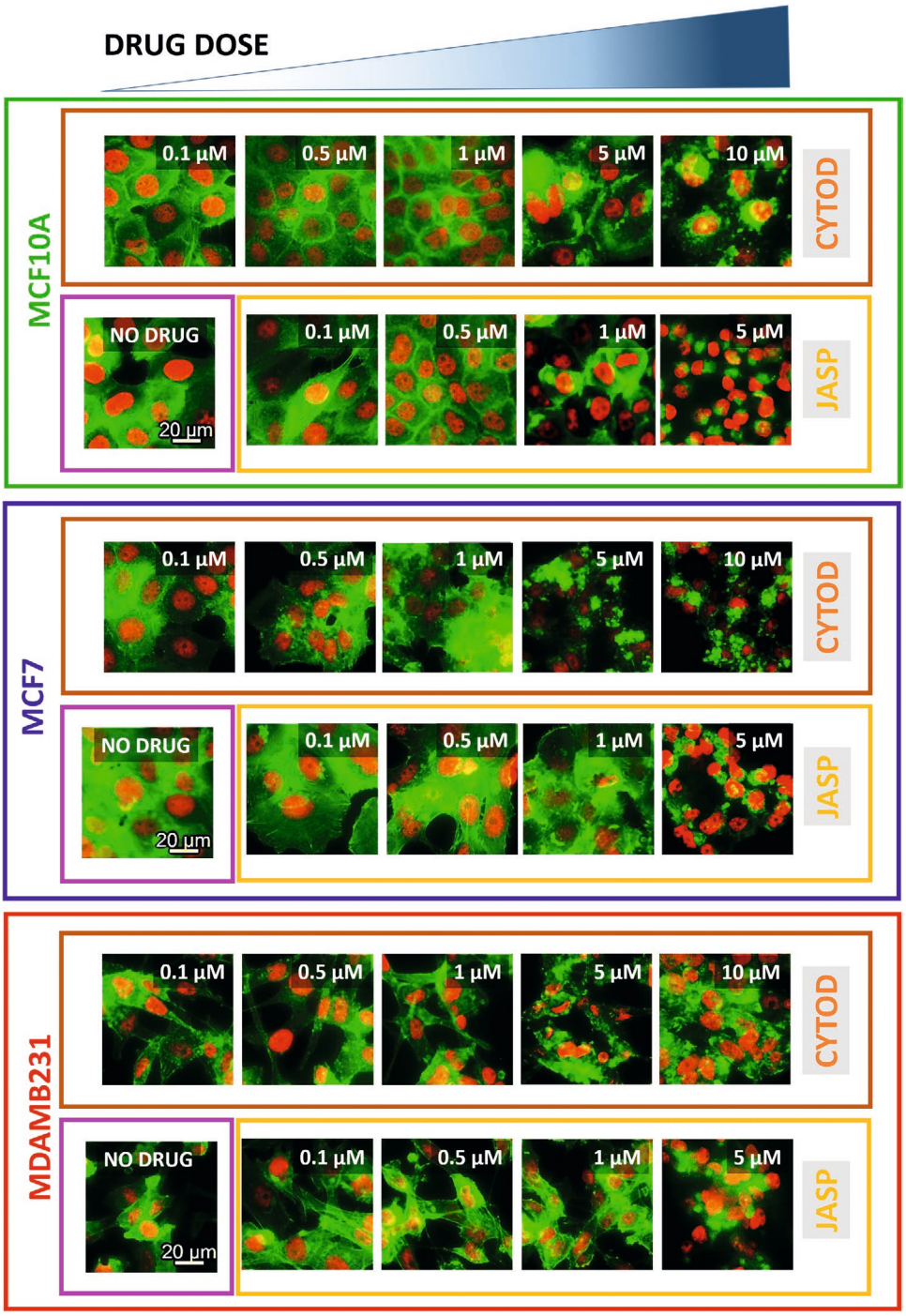


**Figure 2.** Fluorescence microscopy images on the effect of concentration of the drugs (Cytochalasin D (CytoD) and Jasplakinolide (Jasp)) on actin cytoskeleton formation (green: Alexa Fluor 488 Phalloidin) of the three breast cancer cells on TCPS (nucleus: red (DAPI), Scale bar: 20 $\mu$m).

The lower rows show the cells after drug treatment (drug free 24 h incubation followed by 24 h with the drug). After 24 h without the drugs the nuclei of benign cells (MCF10A) were not deformed whereas nuclei of malignant cells MCF7 and MDAMB231 were highly deformed. After 48 h of drug-free incubation, nuclei of all the cell types, regardless of being benign or malignant, were deformed. Thus, the malignant cell types were deformed earlier than the benign ones on micropatterned surfaces.

However, after 24 h incubation with the CytoD (drug free 24 h incubation followed by 24 h with the drug), the nuclei of benign cells were less deformed (MCF10A) while malignant cells were not deformed at all (MCF7 and MDAMB231). With Jasp, on the other hand, the nuclear deformation of the cells was decreased MCF10A and MCF7 but this decrease was significant only for MDAMB231. Thus, CytoD was more effective than Jasp in decreasing the deformability of the cells. It is also

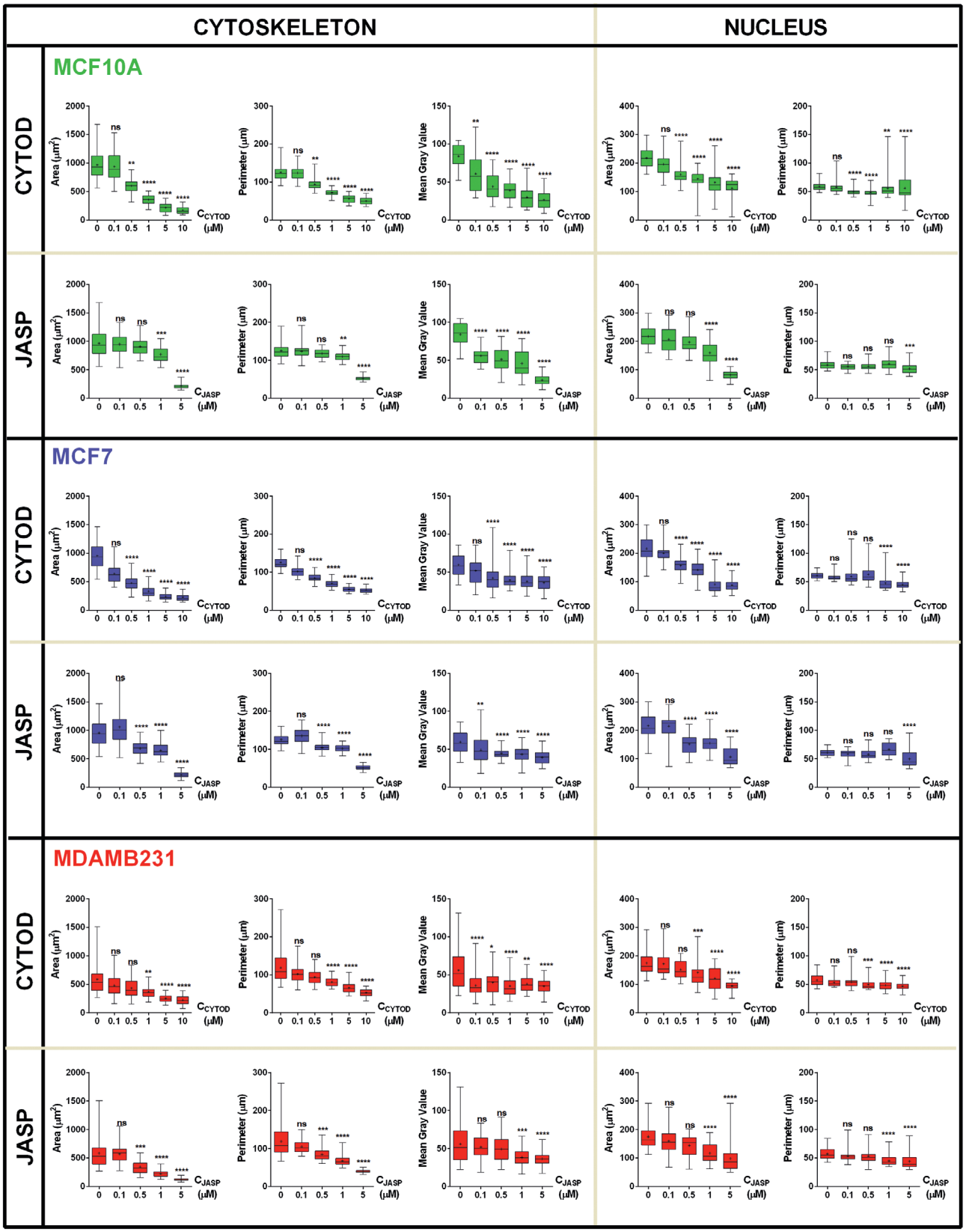


**Figure 3.** Cytoskeletal and nuclear image analysis of three breast cancer cells with the increasing drug concentrations. Two drugs were used (CytoD and Jasp). Area, perimeter, and mean gray value parameters were used for cytoskeletal analysis whereas area and perimeter were used for the nuclei (one-way ANOVA followed by Kruskal–Wallis test, $n \geq 100$, $p < 0.0001$, *$p < 0.005$, **$p < 0.001$, ***$p < 0.0005$, and ****$p < 0.0001$, ns: nonsignificant).

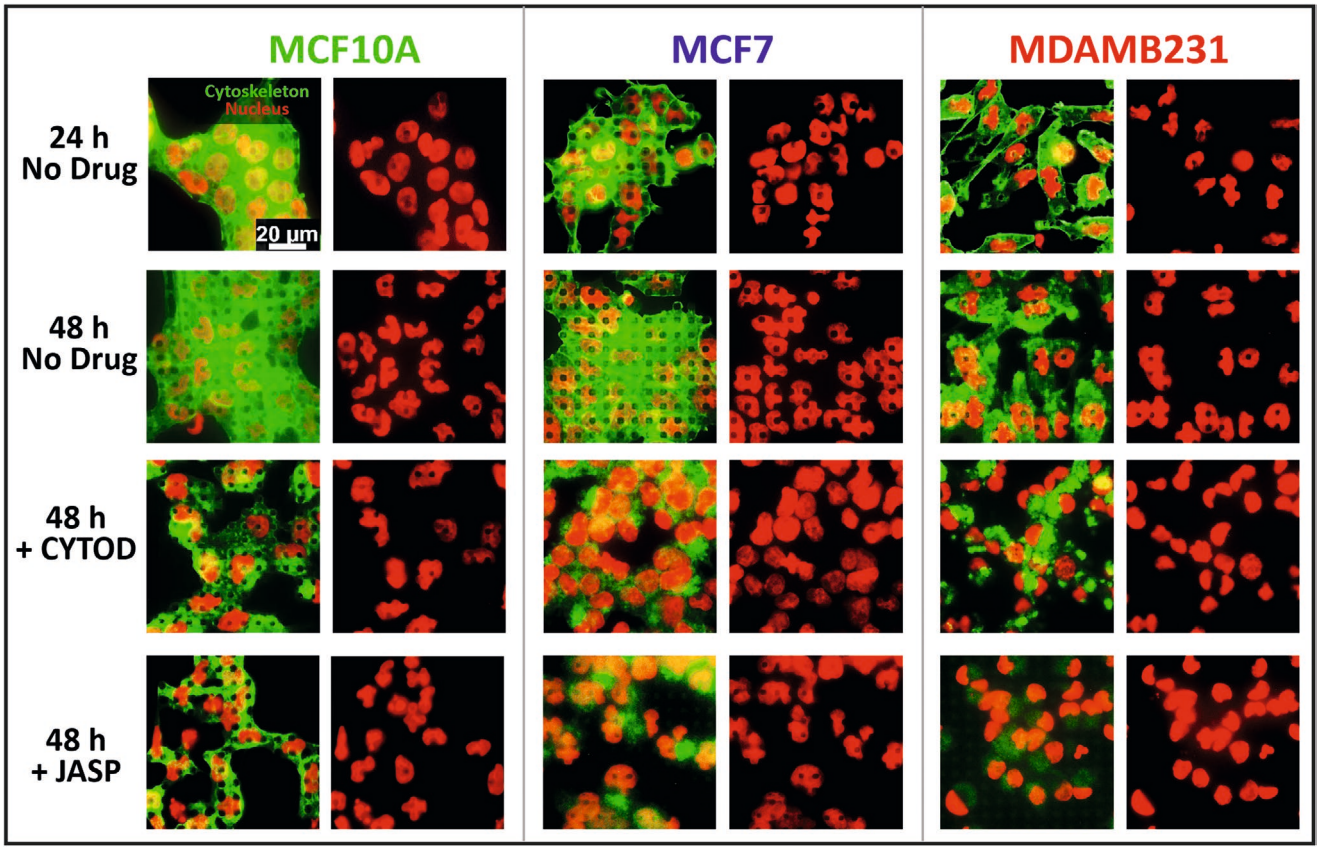


**Figure 4.** Fluorescence microscopy images show the effect of drugs (CytoD, $10 \times 10^{-6}$ M and Jasp, $5 \times 10^{-6}$ M) on actin cytoskeleton by the decrease in the green signal of actin specific stain (Alexa Fluor 488 Phalloidin) and nuclear deformation (DAPI, red) of cells on micropatterned PMMA surfaces after 24 and 48 h without drug (upper two rows) and 48 h after drug treatment (bottom two rows) (Scale bar: 20 $\mu$m).

observed in the images that the drugs disrupted the actin filaments of the cells and simultaneously the nuclear deformations were decreased or lost. This shows that nuclear deformability is directly related to the organization of actins. Studies showed that loss or disruption of actins caused loss of actin-myosin contractility and undeformed, force-free state of cells.[42,44] It was also stated in a review that the actomyosin network is responsible for contractility and force generation in the cell and coordination between the mechanosensors (integrins) and response elements (actin cytoskeleton) guides force transduction and the deformability of the cell.[39] This supports the observation of loss of deformability after disruption of actin filaments in our study.

### 3.2. Quantification of Nuclear Deformation of Cells

Extent of deformation of the cell nuclei was quantified by digital analysis of the fluorescence microscopy images using Fiji software. As a measure of deformation, certain dimensional properties of the cells were employed. Circularity is one such parameter and is a measure of how close a cell nucleus is to a perfect circle. A circularity of 1 indicates a perfect circle whereas a zero is a substantially elongated shape. The equation defining the circularity is presented in Section 2.5.1.

Circularity values of the nuclei of the three cells on micropatterned PMMA surfaces before and after the treatment with CytoD and Jasp are presented in **Figure 5**.

On smooth (unpatterned) surfaces, circularity values for all cells were around 0.8 which is almost a perfect circle value indicating that there is no nuclear deformation.

On micropatterned surfaces, after 24 h, circularity values were 0.78, 0.46, and 0.39 for MCF10A, MCF7, and MDAMB231 cells, respectively. This means that the nuclei of benign MCF10A cells had almost no conformational change whereas nuclei of the cancer cells were severely deformed. Increase in the nuclear deformation by the increase in the malignancy of cells also correlates well with the overall stiffness of the cells and their nuclei obtained in a study.[45] In the literature, Young's modulus values were found to be 0.7, 0.5, and 0.3 kPa for MCF10A, MCF7, and MDAMB231 cells, respectively, supporting the studies reporting that the softest cancer cells were also most deformed on the micropatterned surfaces.[10,13,38] After 48 h, nuclei of all cells were deformed somewhat more; circularity values were now 0.55, 0.41, and 0.37 for MCF10A, MCF7, and MDAMB231, respectively. Results show that eventually, all the cells are deformed but the deformation was slower for benign (MCF10A) cells whereas nuclei of invasive malignant (MDAMB231) cell deformed at a much higher rate. These results were very similar to the results reported earlier

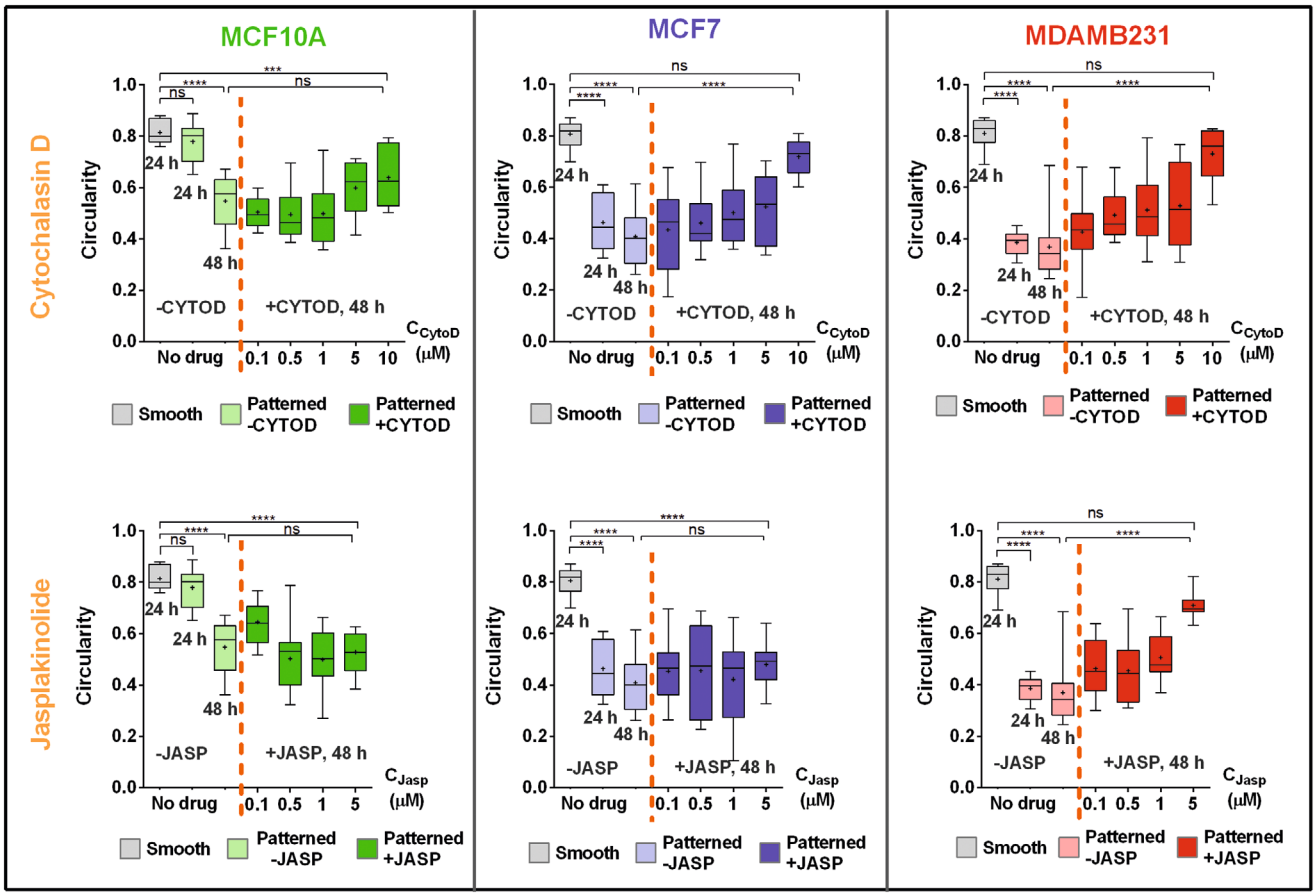


**Figure 5.** Quantification of nuclear deformation by the circularity value calculated from fluorescence microscopy images of the three breast cancer cells before and after CytoD ($10 \times 10^{-6}$ M) and Jasp ($5 \times 10^{-6}$ M) treatment (one-way ANOVA followed by Kruskal–Wallis test, $n \geq 100$, $p < 0.0001$; *$p <$ 0.005, **$p < 0.001$, ***$p < 0.0005$, and ****$p < 0.0001$, ns: nonsignificant).

on the discrimination of breast cancer cells by their malignancies on micropatterned surfaces.[16]

In the tests for drugs acting on actin polymerization and organization, the cells were treated with CytoD and Jasp and then nuclear deformations of the cells were quantified as above.

After the treatment of cells with CytoD concentrations in the range 0.1–10 $\times 10^{-6}$ M, circularity values of all cells increased with an increase in the drug concentration and approached 1.0 even though they were on micropatterned surfaces. The circularity values after the treatment with the highest concentration ($10 \times 10^{-6}$ M) of CytoD were 0.64, 0.72, and 0.73 for MCF10A, MCF7, and MDAMB231, respectively. Benign (MCF10A) cells were not affected by the drug treatment as much as malignant cells (MCF7 and MDAMB231). Malignant cells lost deformability completely upon treatment with the high dose of drug.

When the same test was performed with Jasp (0.1–5 $\times 10^{-6}$ M), only the nuclei of the most malignant cell line, MDAMB231, were affected with a significant increase in the circularity (decrease in the deformation). The circularity values of the three cells after the highest concentration of Jasp ($5 \times 10^{-6}$ M) were 0.53, 0.48, and 0.71 for MCF10A, MCF7, and MDAMB231, respectively.

It is known that actin cytoskeleton of cells not only provides structural support but also defines the mechanical properties of the cells. Actin network is involved in the maintenance of nuclear stiffness and actin filaments are needed for the cell relaxation.[29,30] Thus, in our study, after the disruption of the actin cytoskeleton by the drugs, cells lost their actomyosin contractility and this resulted in the changes observed in their deformability. It can be concluded that there is a direct connection between nuclear deformation and actin filaments of the cells.

### 3.3. Expression of Lamin A/C and Nesprin-2 before and after Drug Treatment

Nuclear envelope (NE) is composed of two distinct lipid bilayers as the inner (INM) and the outer (ONM) nuclear membrane. NE proteins are integrated in the INM (such as emerin and SUN proteins) or in the ONM such as nesprins.[46] Additionally, adjacent to the INM, the nuclear lamina that is composed of Lamin A and C, completes NE composition.[46] These proteins provide integrity of nuclear envelope and constitute the connection between cytoplasmic cytoskeletons networks (such as microtubules and actin) and the genome through the heterochromatin connected to the transduction pathway proteins. Among all the proteins of mechanotransduction, lamins and nesprins are more crucial in disease state of the cell since they were reported as associated with congenital diseases

including cardiac and muscular diseases.[46,47] Thus, they are good targets to study the deformability of a cancer cell. Moreover, Nesprin-2 is directly connected to actin filaments of the cells and Lamin A/C is connected to the chromatin, thus they are important targets to study the effect of forces generated by the cytoskeleton, crossing the nuclear membrane and affecting the transcriptional state of the cell. Thus, Nesprin-2 and Lamin A/C were chosen as cytoplasmic and nuclear components, respectively, to represent the proteins of the transduction pathways.

In addition to the congenital diseases, Lamin A/C and Nesprin-2 also play a role in cancer progression. For instance, they are known to be downregulated in human breast cancer cells.[48] Moreover, they play crucial roles in nuclear membrane organization and mechanical stiffness in breast cancer cells and their downregulation leads to decrease of nuclear and cellular rigidity and increase of tissue fluidity which is a crucial property of malignant cancer cells.[48]

Thus, in this study, Lamin A/C and Nesprin-2 were determined at gene and protein levels with three different methods. At the gene level, RT-qPCR and at the protein level, ICC staining and Western blotting were used. For RT-qPCR and ICC staining, only MCF7 malignant cells were used as a model, and for the Western blotting, all three cells lines were studied.

RT-qPCR results and the experimental details are presented in Figure S8 (Supporting Information). The results for both Lamin A/C and Nesprin-2 showed decreased gene expression levels on micropatterned surfaces compared to that on TCPS and smooth PMMA surfaces before drug treatment. On TCPS and smooth PMMA surfaces, the expression levels of both genes did not show any change indicating any effect of the material.

ICC results are presented in **Figure 6**. Cytoskeletal and nuclear morphologies of MCF7 cells were recorded with CLSM after 24 h incubation in the culture medium followed by another 24 h with the drug CytoD. Images on micropatterned surfaces are presented in Figures 6A,B whereas those on smooth and TCPS surfaces are presented in Figures S6 and S7 (Supporting Information). Protein expression levels were calculated from the intensity of the stains in the confocal microscopy images (Figure 6C,D). Before drug addition images show that nuclei of MCF7 cells are deformed on P4G4 micropatterned surfaces (Figure 6A,B, first rows). After the addition of drug CytoD, the actin cytoskeletons of the cells were disrupted as shown by the actin specific stain (green: Alexa Fluor 532 Phalloidin) and the nuclear deformability of the cells were lost on micropatterned surfaces (Figure 6A,B, second rows). However, signal intensities of both Lamin A/C and Nesprin-2 were increased (blue: Anti Lamin A or Anti-Nesprin-2) (Figure 6C,D) as was measured and quantified with ImageJ (NIH) software. Results were optimized by the cell number; signal intensities were divided by the number of cells on the same surface. The results show that after drug treatment, simultaneously with loss of nuclear deformability signal intensities of Lamin A/C and Nesprin-2 were increased on patterned surfaces (Figure 6C,D). This indicates that their expression levels were increased. On TCPS and smooth surfaces, on the other hand, intensities of the proteins did not change significantly, and nuclear deformation was not observed.

Western blot results are presented in **Figure 7**. Western blot analysis was applied to determine expression levels of both Lamin A/C and Nesprin-2 proteins before and after drug (CytoD, $10 \times 10^{-6}$ M) addition on patterned and smooth PMMA and TCPS surfaces. The results show that on patterned surfaces, expression of both proteins increased after drug treatment similar to the ICC results. However, this increase was not significant in MCF10A and MCF7 cells while it was highly significant in the most malignant cells, MDAMB231. In immunocytochemistry staining analysis, MCF7 cells also showed a significant increase in the expression level of two proteins after drug treatment. However, in Western blot analysis, the changes in the protein expression levels of different groups were not significant. It may be a result of the sensitivity of the two methods (ICC vs Western blot). On smooth and TCPS surface, protein levels before and after drug treatment did not change much and the results were not statistically significant.

The results obtained by the three methods (RT-qPCR, ICC, Western blot) mostly correlate and they all show that especially in malignant cells, with the disruption of actin filaments, nuclear deformation decreased, and expression of Lamin A/C and Nesprin-2 proteins increased on patterned surfaces. The reason of the loss of deformation can be explained with the need of actomyosin contractility for the movement and dislocation of the cells and their nuclei.[49–51] Lamin A/C and Nesprin-2 directly interact with actin filaments of the cells. CytoD caused the disruption of actin filament formation by inhibiting their polymerization, and therefore, cells lost actomyosin contractility, the transfer of mechanobiological stimuli is hampered and therefore, deformability is decreased. Data from the literature support the existence of a relation between the actin filaments polymerization and deformation of nucleus. For example, a recent study reported that when dendritic cells were forced to pass through micrometric constrictions, actin polymerization around the nucleus was required for the cells since these fibers are involved in actomyosin contractility and force transduction in the cell which start from the cell membrane and end up with the nucleus.[49] Moreover, it was shown that Lamin A/C and B proteins form a rigid structure at the inner nuclear membrane and cells need to express less lamin gene product to be able to migrate.[49] Moreover, in a different study, a single living cell compression device was used and wild-type and LMNA knockout mouse embryonic fibroblasts were compared in terms of their stiffness. It was reported that LMNA knockout cells showed a significantly decreased mechanical stiffness.[52] In another study, Lamin A to B ratio of three different cells (glioblastoma U251 cells, lung carcinoma A549 cells, bone marrow mesenchymal stem cells) with varying stiffnesses was compared and it was reported that the softer cells presented lower Lamin A levels.[53] Moreover, in a recent study, authors created different cytoskeletal shapes in mouse fibroblasts using micropatterned substrates and they studied the alterations in nuclear deformability in response to actin, myosin, formin perturbations, and the transcriptional downregulation of lamin A/C levels. They concluded that active forces from the cytoskeleton and rigidity of lamin A/C nucleoskeleton can regulate nuclear deformability of the cells.[54] All these studies show that deformable and softer cancer cells had lower Lamin A/C protein expres-

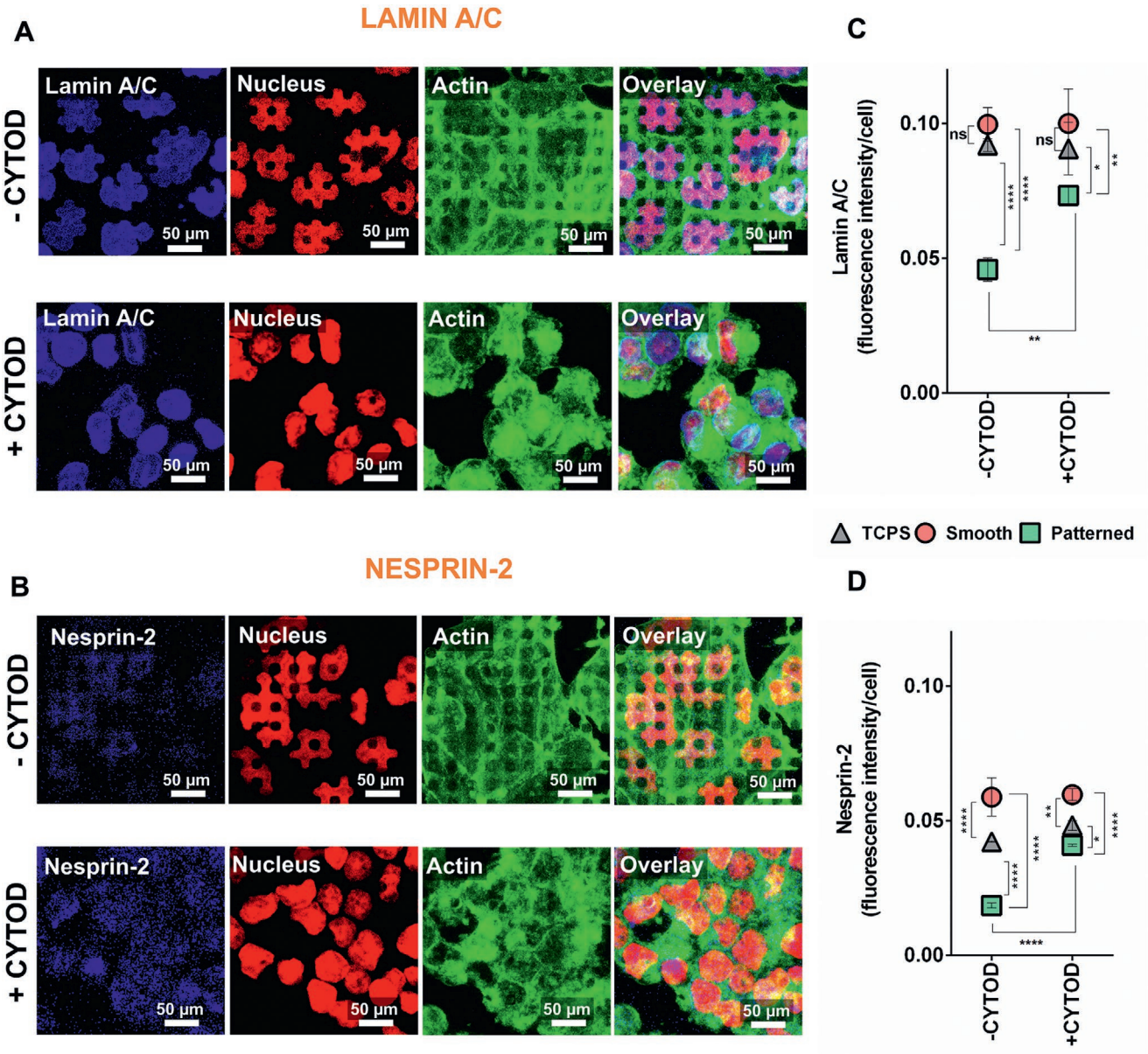


**Figure 6.** ICC staining of MCF7 malignant breast cancer cells with Lamin A/C and Nesprin-2 specific antibodies. CLSM images of cells on micropatterned surfaces stained for A) Lamin A/C and B) Nesprin-2 (blue: Anti Lamin A or Anti-Nesprin-2), nucleus (red: TOPRO-3) and actin filaments (green: Alexa Fluor 532 Phalloidin) (40× objective, Scale bars: 50 $\mu$m). Quantification of expression levels of C) Lamin A/C and D) Nesprin-2 before and after drug treatment as determined from their fluorescence intensities on micropatterned, smooth, and TCPS surfaces. Fluorescence intensities were calculated using ImageJ (NIH) software. Results were given as dividing signal intensities by the number of cells counted from the same surface (two-way ANOVA followed by Sidak's multiple comparison test, $n = 3$, $p_{\text{LaminA/C}} = 0.0092$, $p_{\text{Nesprin-2}} = 0.0002$; $^{*}p < 0.005$, $^{**}p < 0.001$, $^{***}p < 0.0005$, and $^{****}p < 0.0001$, ns: nonsignificant).

sions. In another study, it was reported that nesprins served as linkers of actin cytoskeleton to the nuclear envelope and had an important role in controlling nucleus positioning.[50] Furthermore, it was shown that when nesprins were knockdown in osteosarcoma cells, their nuclear deformability was decreased which proved the essential role of nesprins in actomyosin contractility and nucleo-cytoskeletal connections.[51] In summary, based on the results and the literature data, we confirm that in addition to the actin cytoskeleton, nuclear envelope protein Lamin A/C and LINC protein Nesprin-2 have fundamental roles in nuclear localization and in intercellular interactions between inner nuclear and outer cytoskeletal components of the cells.

## 4. Conclusion

Cancerous and healthy cells have differences in their flexibility due to their biomechanical properties. They reflect these differences more clearly when placed on micropatterned

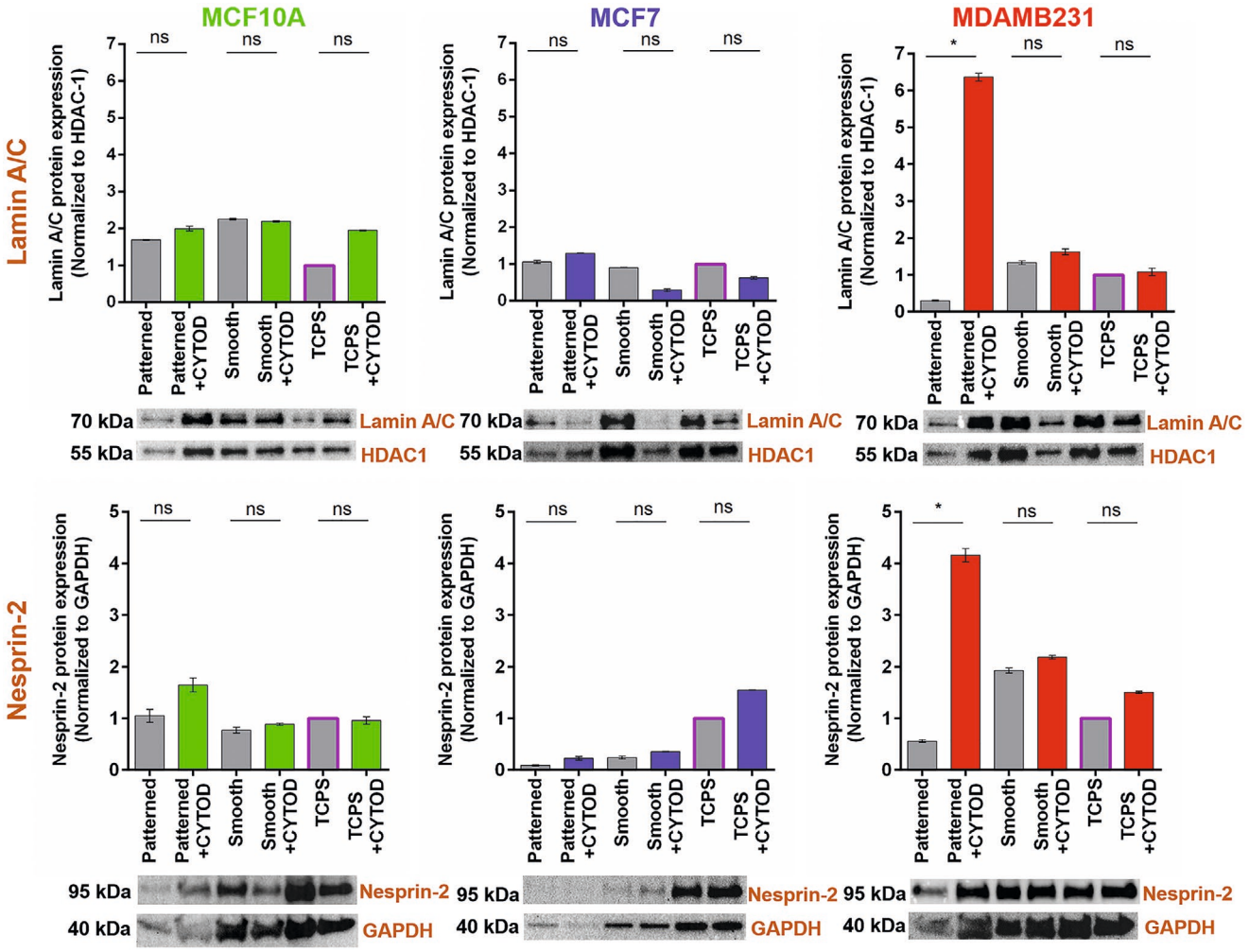


**Figure 7.** Western blot analysis of Lamin A/C and Nesprin-2 proteins in three breast cancer cell lines are presented before and after drug (+CytoD, $10 \times 10^{-6}$ M) treatment on patterned and smooth PMMA and TCPS. Full-sized immunoblot images are given in Figure S10 (Supporting Information). Protein expression levels on TCPS surface without drug treatment are used as control to calculate relative changes in the protein expressions. All results are normalized to GAPDH and HDAC-1 housekeeping genes for cytoplasmic and nuclear proteins, respectively (one-way ANOVA followed by Kruskal–Wallis test, $n \geq 100$, $p_{MCF10A/LaminA/C} = 0.0005$, $p_{MCF7/LaminA/C} < 0.0001$, $p_{MDAMB231/LaminA/C} < 0.0001$, $p_{MCF10A/Nesprin\text{-}2} = 0.0126$, $p_{MCF7/Nesprin\text{-}2} = 0.0004$, $p_{MDAMB231/Nesprin\text{-}2} < 0.0001$; $*p < 0.005$, $**p < 0.001$, $***p < 0.0005$, and $****p < 0.0001$, ns: nonsignificant).

surfaces instead of smooth. Deformability is one such property that is expressed more by cancerous or diseased cells. It is important to study the underlying molecular mechanism of this mechanobiological difference. Deformability carries hints about the metastatic capability and the malignancy of the cells. Thus, in this study, micropatterned surfaces served as imaging and screening tools for the morphological properties of three breast cancer cell lines with different malignancy levels. Application of actin polymerization inhibiting drugs led to substantial decrease of nuclear deformation. This was supported by an increase in the expression of Lamin A/C and Nesprin-2 proteins. As a result, actin inhibiting drugs showed that actin filament integrity and Lamin A/C and Nesprin-2 protein levels are correlated and have distinct roles in force transmission and nuclear deformation of the cells. These also revealed that nuclear deformation level can be a clue about the metastatic property of cancer cells and micropatterned surfaces facilitate the expression of this property.

## Supporting Information

Supporting Information is available from the Wiley Online Library or from the author.

## Acknowledgements

E.A. and V.H. acknowledge the Middle East Technical University (METU), Center of Excellence in Biomaterials and Tissue Engineering (BIOMATEN) for the use of the facilities and METU Central Laboratory for SEM analyses. The authors thank Dr. Menekse Ermis Sen and Cagdas Ermis for their contribution in western blot analysis. E.A. and V.H. acknowledge the Ministry of Development of Turkey, METU BAP-01-08-2013-003 and BAP-08-11-DPT2011K120350, METU BIOMATEN and TUBITAK 2211-C scholarship. U.D. would also like to acknowledge Canary Foundation seed grant, NCI Center for Cancer Nanotechnology Excellence for Translational Diagnostics (NIH NCI U54CA199075).

## Conflict of Interest

The authors E.A. and V.H. declare no conflict of interest. U.D. is a founder of, and has an equity interest in: i) DxNow Inc., a company that is developing microfluidic and imaging technologies for point-of-care diagnostic solutions, ii) Koek Biotech, a company that is developing microfluidic IVF technologies for clinical solutions, and iii) Levitas Inc., a company that is developing magnetic levitation tools. U.D.'s interests were viewed and managed in accordance with the conflict of interest policies.

## Author Contributions

The manuscript was written through the contributions of all authors. All authors have approved the final version of the manuscript.

## Keywords

actin filaments, breast cancer, mechanotransduction, micropattern, nuclear deformation

Received: February 12, 2020
Revised: October 16, 2020
Published online: December 23, 2020

[1] M. J. Dalby, *Med. Eng. Phys.* **2005**, *27*, 730.
[2] K. Ohashi, S. Fujiwara, K. Mizuno, *J. Biochem.* **2017**, *161*, 245.
[3] D. A. Fletcher, R. D. Mullins, *Nature* **2010**, *463*, 485.
[4] N. M. Ramdas, G. V. Shivashankar, *J. Mol. Biol.* **2015**, *427*, 695.
[5] J. M. Northcott, I. S. Dean, J. K. Mouw, V. M. Weaver, *Front. Cell Dev. Biol.* **2018**, *6*, 17.
[6] D.-H. Kim, J. Hah, D. Wirtz, in *Biomechanics in Oncology, Advances in Experimental Medicine and Biology*, Vol. *1092*, Springer, New York **2018**, pp. 41–55.
[7] K. N. Dahl, S. M. Kahn, K. L. Wilson, D. E. Discher, *J. Cell Sci.* **2004**, *117*, 4779.
[8] Y. Tseng, J. S. H. Lee, T. P. Kole, I. Jiang, D. Wirtz, *J. Cell Sci.* **2004**, *117*, 2159.
[9] A. H. Mekhdjian, F. B. Kai, M. G. Rubashkin, L. S. Prahl, L. M. Przybyla, A. L. McGregor, E. S. Bell, J. M. Barnes, C. C. DuFort, G. Ou, A. C. Chang, L. Cassereau, S. J. Tan, M. W. Pickup, J. N. Lakins, X. Ye, M. W. Davidson, J. Lammerding, D. J. Odde, A. R. Dunn, V. M. Weaver, *Mol. Biol. Cell* **2017**, *28*, 1467.
[10] P. M. Davidson, C. Denais, M. C. Bakshi, J. Lammerding, *Cell. Mol. Bioeng.* **2014**, *7*, 293.
[11] M. J. Mitchell, C. Denais, M. F. Chan, Z. Wang, J. Lammerding, M. R. King, *Am. J. Physiol.* **2015**, *309*, C736.
[12] A. M. Greiner, A. Sales, H. Chen, S. A. Biela, D. Kaufmann, R. Kemkemer, *Beilstein J. Nanotechnol.* **2016**, *7*, 1620.
[13] M. Ermis, D. Akkaynak, P. Chen, U. Demirci, V. Hasirci, *Sci. Rep.* **2016**, *6*, 36917.
[14] O. Hasturk, A. Sivas, B. Karasozen, U. Demirci, N. Hasirci, V. Hasirci, *Adv. Healthcare Mater.* **2016**, *5*, 2972.
[15] E. Antmen, M. Ermis, U. Demirci, V. Hasirci, *J. Biomed. Mater. Res., Part B* **2019**, *107*, 366.
[16] E. Antmen, U. Demirci, V. Hasirci, *Colloids Surf., B* **2019**, *183*, 110402.
[17] R. G. Flemming, C. J. Murphy, G. A. Abrams, S. L. Goodman, P. F. Nealey, *Biomaterials* **1999**, *20*, 573.
[18] A. S. G. Curtis, M. Dolby, N. Gadegaand, *Nanomedicine* **2006**, *1*, 67.
[19] V. Hasirci, H. Kenar, *Nanomedicine* **2006**, *1*, 73.
[20] K. Matsuzaka, X. F. Walboomers, M. Yoshinari, T. Inoue, J. A. Jansen, *Biomaterials* **2003**, *24*, 2711.
[21] J. B. Recknor, J. C. Recknor, D. S. Sakaguchi, S. K. Mallapragada, *Biomaterials* **2004**, *25*, 2753.
[22] P. Clark, P. Connolly, A. S. G. Curtis, J. A. Dow, C. D. Wilkinson, *Development* **1987**, *99*, 439.
[23] P. Clark, P. Connolly, A. S. G. Curtis, J. A. T. Dow, C. D. W. Wilkinson, *Development* **1990**, *108*, 635.
[24] B. Wójciak-Stothard, A. Curtis, W. Monaghan, K. Macdonald, C. Wilkinson, *Exp. Cell Res.* **1996**, *223*, 426.
[25] B. G. Keselowsky, L. Wang, Z. Schwartz, A. J. Garcia, B. D. Boyan, *J. Biomed. Mater. Res., Part A* **2007**, *80A*, 700.
[26] C. S. Chen, M. Mrksich, S. Huang, G. M. Whitesides, D. E. Ingber, *Science* **1997**, *276*, 1425.
[27] F. M. Watt, P. W. Jordan, C. H. O'Neill, *Proc. Natl. Acad. Sci. USA* **1988**, *85*, 5576.
[28] A. Bruinink, E. Wintermantel, *Biomaterials* **2001**, *22*, 2465.
[29] H. Kubitschke, J. Schnauss, K. D. Nnetu, E. Warmt, R. Stange, J. Kaes, *New J. Phys.* **2017**, *19*, 093003.
[30] B. Xuan, D. Ghosh, E. M. Cheney, E. M. Clifton, M. R. Dawson, *Sci. Rep.* **2018**, *8*, 11935.
[31] C. T. Rueden, J. Schindelin, M. C. Hiner, B. E. DeZonia, A. E. Walter, E. T. Arena, K. W. Eliceiri, *BMC Bioinf.* **2017**, *18*, 529.
[32] N. Phansalkar, S. More, A. Sabale, M. Joshi, in *ICCSP 2011, 2011 Int. Conf. Commun. Signal Process.*, IEEE, Piscataway, NJ **2011**, pp. 218–220.
[33] J. Schindelin, I. Arganda-Carreras, E. Frise, V. Kaynig, M. Longair, T. Pietzsch, S. Preibisch, C. Rueden, S. Saalfeld, B. Schmid, J. Y. Tinevez, D. J. White, V. Hartenstein, K. Eliceiri, P. Tomancak, A. Cardona, *Nat. Methods* **2012**, *9*, 676.
[34] S. R. Sternberg, *Computer* **1983**, *16*, 22.
[35] M. Lekka, P. Laidler, D. Gil, J. Lekki, Z. Stachura, A. Z. Hrynkiewicz, *Eur. Biophys. J.* **1999**, *28*, 312.
[36] P. Friedl, K. Wolf, J. Lammerding, *Curr. Opin. Cell Biol.* **2011**, *23*, 55.
[37] H. Huang, J. Sylvan, M. Jonas, R. Barresi, P. T. C. So, K. P. Campbell, R. T. Lee, *Am. J. Physiol.* **2005**, *288*, C72.
[38] J. Chen, D. Weihs, M. Van Dijk, F. J. Vermolen, *Biomech. Model. Mechanobiol.* **2018**, *17*, 1429.
[39] C. C. Dufort, M. J. Paszek, V. M. Weaver, *Nat. Rev. Mol. Cell Biol.* **2011**, *12*, 308.
[40] O. Otto, P. Rosendahl, A. Mietke, S. Golfier, C. Herold, D. Klaue, S. Girardo, S. Pagliara, A. Ekpenyong, A. Jacobi, M. Wobus, N. Töpfner, U. F. Keyser, J. Mansfeld, E. Fischer-Friedrich, J. Guck, *Nat. Methods* **2015**, *12*, 199.
[41] H. L. Glenn, J. Messner, D. R. Meldrum, *Sci. Rep.* **2016**, *6*, 31694.
[42] J. Shankar, I. R. Nabi, *PLoS One* **2015**, *10*, e0119954.
[43] C. Hayot, O. Debeir, P. Van Ham, M. Van Damme, R. Kiss, C. Decaestecker, *Toxicol. Appl. Pharmacol.* **2006**, *211*, 30.
[44] T. M. Koch, S. Münster, N. Bonakdar, J. P. Butler, B. Fabry, *PLoS One* **2012**, *7*, e33476.
[45] A. Calzado-Martín, M. Encinar, J. Tamayo, M. Calleja, A. San Paulo, *ACS Nano* **2016**, *10*, 3365.
[46] A. Janin, V. Gache, *Front. Physiol.* **2018**, *9*, 1277.
[47] M. L. Lombardi, D. E. Jaalouk, C. M. Shanahan, B. Burke, K. J. Roux, J. Lammerding, *J. Biol. Chem.* **2011**, *286*, 26743.
[48] A. Matsumoto, M. Hieda, Y. Yokoyama, Y. Nishioka, K. Yoshidome, M. Tsujimoto, N. Matsuura, *Cancer Med.* **2015**, *4*, 1547.
[49] H.-R. Thiam, P. Vargas, N. Carpi, C. L. Crespo, M. Raab, E. Terriac, M. C. King, J. Jacobelli, A. S. Alberts, T. Stradal, A.-M. Lennon-Dumenil, M. Piel, *Nat. Commun.* **2016**, *7*, 10997.
[50] I. Dupin, Y. Sakamoto, S. Etienne-Manneville, *J. Cell Sci.* **2011**, *124*, 865.
[51] N. T. Wakhloo, S. Anders, F. Badique, M. Eichhorn, I. Brigaud, T. Petithory, M. Vassaux, J. L. Milan, J. N. Freund, J. Rühe,

P. M. Davidson, L. Pieuchot, K. Anselme, *Biomaterials* **2020**, *234*, 119746.

[52] J. L. V. Broers, E. A. G. Peeters, H. J. H. Kuijpers, J. Endert, C. V. C. Bouten, C. W. J. Oomens, F. P. T. Baaijens, F. C. S. Ramaekers, *Hum. Mol. Genet.* **2004**, *13*, 2567.

[53] T. Harada, J. Swift, J. Irianto, J. W. Shin, K. R. Spinler, A. Athirasala, R. Diegmiller, P. C. D. P. Dingal, I. L. Ivanovska, D. E. Discher, *J. Cell Biol.* **2014**, *204*, 669.

[54] E. Makhija, D. S. Jokhun, G. V. Shivashankar, *Proc. Natl. Acad. Sci. USA* **2016**, *113*, E32.